17

INPUT RESISTANCE, TIME CONSTANTS, AND SPIKE INITIATION

This chapter represents somewhat of a technical interlude. Having introduced the reader to both simplified and more complex compartmental single neuron models, we need to revisit terrain with which we are already somewhat familiar.

In the following pages we reevaluate two important concepts we defined in the first few chapters: the somatic *input resistance* and the neuronal *time constant*. For passive systems, both are simple enough variables: R_{in} is the change in somatic membrane potential in response to a small sustained current injection divided by the amplitude of the current injection, while τ_m is the slowest time constant associated with the exponential charging or discharging of the neuronal membrane in response to a current pulse or step. However, because neurons express nonstationary and nonlinear membrane conductances, the measurement and interpretation of these two variables in active structures is not as straightforward as before. Having obtained a more sophisticated understanding of these issues, we will turn toward the question of the existence of a current, voltage, or charge threshold at which a biophysical faithful model of a cell triggers action potentials. We conclude with recent work that suggests how concepts from the subthreshold domain, like the input resistance or the average membrane potential, could be extended to the case in which the cell is discharging a stream of action potentials.

This chapter is mainly for the cognoscendi or for those of us that need to make sense of experimental data by comparing them to theoretical models that usually fail to reflect reality adequately.

17.1 Measuring Input Resistances

In Sec. 3.4, we defined $\tilde{K}_{ii}(f)$ for passive cable structures as the voltage change at location i in response to a sinusoidal current injection of frequency f at the same location. Its

dc component is also referred to as input resistance or R_{in}. Three difficulties render this definition of input resistance problematic in real cells: (1) most membranes, in particular at the soma, show voltage-dependent nonlinearities, (2) the associated ionic membrane conductances are time dependent and (3) instrumental aspects, such as the effect of the impedance of the recording electrode on R_{in}, add uncertainty to the measuring process. While we will not deal with the last problem (see Smith et al., 1985 for further information). we do have to address the first two issues.

In order to gain a better understanding of the input resistance, we need to focus on the steady-state current-voltage relationship illustrated in Fig. 17.1. $I_{\infty}^{\text{static}}(V_m)$, or sometimes simply $I_{\infty}(V_m)$, is obtained by clamping the membrane potential at the soma to V_m, letting the system adapt and measuring the clamp current flowing across the somatic membrane.

Using the standard Hodgkin-Huxley formalism, we can express the clamp current as

$$I_{\infty}(V_m) = \sum_i g_i(V_m)(V_m - E_{\text{rev,i}}) = \sum_i \overline{g_i} m_{\infty,i}^{a_i} h_{\infty,i}^{b_i}(V_m - E_i) \qquad (17.1)$$

where the summation index i includes all conductances, whether or not they are voltage-dependent (for more details, see Chap. 6). Equation 17.1 does not include an additive term corresponding to the current flowing into or out of the dendrites. Not surprisingly, and

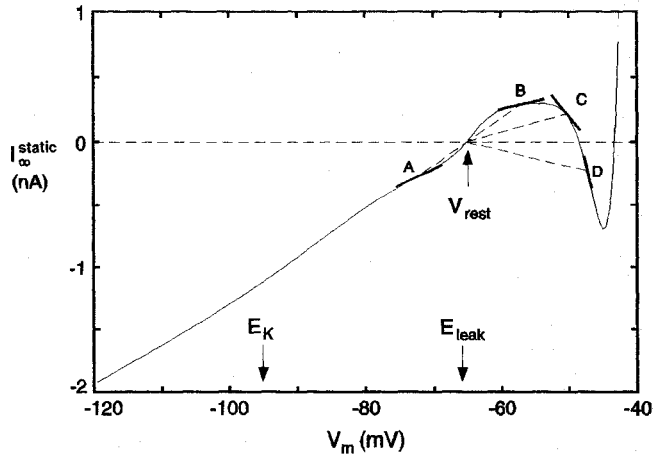

Fig. 17.1 STATIONARY CURRENT-VOLTAGE RELATIONSHIP Stationary I–V relationship for the layer 5 pyramidal cell model of Fig. 3.7. Operationally, $I_{\infty}^{\text{static}}(V_m)$ is measured by clamping the somatic membrane potential to V_m, letting the system adapt and measuring the clamp current flowing across the somatic membrane. The currents to the right of their reversal potentials (indicated by arrows) are outward going, that is, positive. Thus, for $V_m \geq E_K$, all potassium currents are positive while for the entire voltage range shown here, I_{Na} is negative. Typical of excitable cells, the I–V relationship is highly nonlinear, in particular for depolarizing membrane potentials. It intersects the zero current axis at three points. The resting potential of this system, specified by the leftmost zero crossing is $V_{\text{rest}} = -65$ mV. The *chord conductance* is defined as the ratio of the current at any holding potential V_m to the voltage difference between V_m and the resting potential V_{rest}. For points A, B, and C it is positive, and for D, negative. The *slope conductance* is defined as the local tangent to the I–V curve, that is as the slope of the curve. The slope conductance at A and B is positive and at C and D negative. For the linear portion of the I–V curve, the chord conductance is almost identical to the slope conductance (e.g., point A). The inverse of the *slope conductance* is usually what is meant by "input resistance."

different from a linear ohmic resistance, the total somatic membrane current is a nonlinear function of the membrane potential, in particular for depolarizing values. The resting state of the cell is given by the leftward (Fig. 17.1) stable zero crossing at −65 mV.

We can better understand $I_\infty(V_m)$ in Fig. 17.1 by recalling that for any current that can be expressed as the product of a driving potential and a conductance, values of V_m to the left of the associated reversal potential correspond to an inward, that is, negative current. Conversely, holding the potential to a more depolarized value than the reversal potential causes an outward (positive) current to flow.

For example, the long slope to the left of V_{rest} is due to the passive leak conductance and the anomalous rectifier current I_{AR}, the hump between −65 and −48 mV is caused by activation of the delayed-rectifier K^+ current, and the sharp negative peak around −45 mV in Fig. 17.1 by I_{Na}. The large outward current at more positive values of V_m is almost exclusively carried by the noninactivating I_{DR}, overshadowing the inactivating I_{Na}. This I–V curve gives us the opportunity to define two quite different conductances.

17.1.1 Membrane Chord Conductance

The steady-state membrane *chord conductance* is defined as the ratio of the total current flowing at any particular potential V_m to the applied membrane potential relative to the resting potential,

$$G_{\text{in}}^{\text{chord}} = \frac{I_\infty(V_m) - I_\infty(V_{\text{rest}})}{V_m - V_{\text{rest}}} = \frac{I_\infty(V_m)}{V_m - V_{\text{rest}}}. \tag{17.2}$$

The chord conductance derives its name from its construction: conceptually, it can be obtained by pulling a chord or string between the points, $(V_{\text{rest}}, 0)$ and $(V_m, I_\infty(V_m))$. Physically, the chord conductance tells us about the sign and the absolute value of the total membrane current flowing at any one potential. If the I–V relationship has several stable resting points, the chord conductance can be defined around each resting point.

17.1.2 Membrane Slope Conductance

The steady-state membrane *slope conductance* is defined as the local slope of the I–V relationship at the operating point V_m,

$$G_{\text{in}}^{\text{static}} = \frac{dI_\infty^{\text{static}}(V_m)}{dV_m} = \sum_i \left[g_i(V_m) + \frac{dg_i(V_m)}{dV_m}(V_m - E_i) \right] \tag{17.3}$$

(for a single compartmental model). Analytically, the slope conductance corresponds to the linear term in the Taylor series approximation of I_∞^{static} around V_m. The slope conductance of the entire membrane consists of the sum of the individual membrane conductances $g_i(V_m)$ plus a derivative term to account for the membrane nonlinearities.

When using a current pulse to measure $G_{\text{in}}^{\text{static}}$ (Fig. 17.2), one must be careful to wait long enough until all the slow membrane currents have reached equilibrium.

The Inverse of the Slope Conductance Is the Input Resistance

Because the slope conductance characterizes the response of the membrane current to small changes in the membrane potential relative to V_m, its inverse is usually what is meant by *input resistance* R_{in} (which is the convention we will follow). Figure 17.2 illustrates this procedure graphically. Injecting a small current into the soma of the pyramidal cell model causes the membrane potential to peak before it settles down to its final value. Dividing

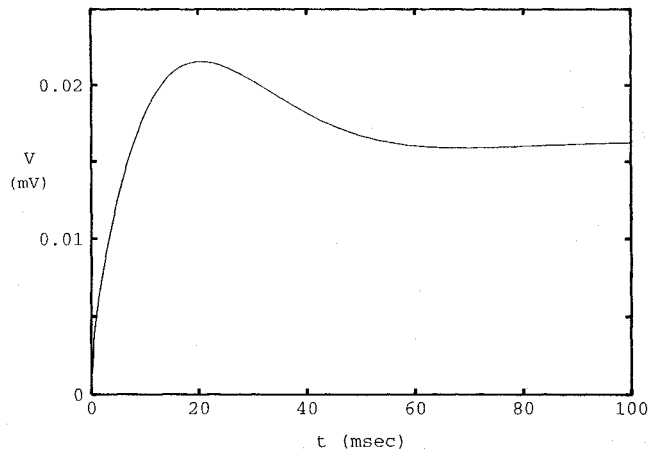

Fig. 17.2 MEASURING THE INPUT RESISTANCE Somatic membrane potential in response to a current step of 1-pA amplitude in the pyramidal cell model. At $V_{\text{rest}} = -65\,mV$, the steady-state slope conductance $G_{\text{in}}^{\text{static}} = 1/0.0165 = 60.6$ nS, corresponding to an input resistance R_{in} of 16.5 MΩ. The initial overshoot is due to activation and subsequent inactivation of the transient A current. Blocking I_{A} causes this hump to disappear and increases R_{in} to 38 MΩ. Reprinted by permission from Bernander (1993).

this steady-state change in potential by the injected current gives the input resistance as 16.5 MΩ. The hump disappears if the transient A current is blocked. Now the potential rises smoothly to its final value.

For a linear I–V relationship the second term in Eq. 17.3 disappears and the slope conductance is equal to the chord conductance and corresponds to $1/\tilde{K}_{ii}$ (e.g., point A in Fig. 17.1). In other words, for linear systems these difficulties with the definition of the input resistance do not arise.

In principle, $G_{\text{in}}^{\text{static}}$ can be measured under either voltage clamp or current clamp. For instance, to compute the slope conductance at rest, we can inject a small current δI into the cell and measure the steady-state voltage change δV (as in Fig. 17.2) or, conversely, we can clamp the potential from V_{rest} to a slightly displaced value $V_{\text{rest}} \pm \delta V$ and measure the change in clamp current δI. For small enough values of δI and δV, both methods converge to the same result.

Negative Slope Conductance

Because the magnitude of the second term in Eq. 17.3 can often be much larger than the first term but of opposite sign, the slope conductance can be negative, zero, or positive. To understand the significance of this, let us look at the example in Fig. 17.3. At rest, the slope conductance at the soma is 57 nS. In the presence of excitatory NMDA synaptic input to the dendritic tree, the soma depolarizes by about 3 mV. Injecting a hyperpolarizing current to bring the membrane potential back to its resting potential now yields a reduced slope conductance of 50.3 nS. Quadrupling the amount of NMDA input drops the slope conductance to 20 nS.

This result appears paradoxical: adding membrane conductance, that is, opening ionic channels, causes a decrease in the local input conductance. It can be explained in a qualitative manner by appealing to Eq. 17.3. (We here gloss over the fact that the NMDA synapses in Fig. 17.3 are distributed throughout the cell, while Eq. 17.3 applies to a single compartment.)

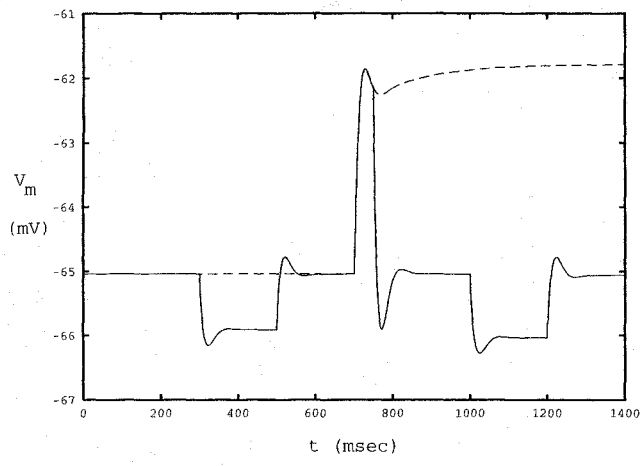

Fig. 17.3 NEGATIVE SLOPE CONDUCTANCE Activating NMDA synapses can lead to a paradoxical *decrease* in the slope conductance $dI_\infty(V_m)/dV_m$. At rest, the slope conductance is 57 nS (as determined by the amplitude of the current step divided by the amplitude of the hyperpolarizing potential after it has converged at around 500 msec). At $t = 700$ msec, synaptic input of the NMDA type that is distributed throughout the dendritic tree is activated, depolarizing the soma by 3 mV (dashed line). Because this shift in the potential activates or inactivates some of the voltage-dependent somatic conductances, confounding the measurement of $dI_\infty(V_m)/dV_m$, the potential is brought back with the help of a hyperpolarizing clamp current (solid line). Repeating the current pulse experiment reveals a slope conductance of 50.3 nS, even though the total membrane conductance has increased with activation of the NMDA synapses.

The first term corresponds to the total amount of NMDA conductance added. This positive term is overwhelmed by the $[dg_i(V_m)/dV_m](V_m - E_i)$ term. Due to the negative slope region of the NMDA receptor (see Fig. 4.8A) and the reversal potential $E_i = 0$, this term is negative and dominates the total conductance in this voltage regime. We shall promptly discuss the relevance of the slope conductance to the spiking threshold.

In our discussion of input conductance, we neglected any temporal aspects of the I–V relationship. Both chord as well as slope conductances can also be defined for the instantaneous I–V relationship or for any other point in time. (For more details see the discussion in Jack, Noble, and Tsien, 1975.)

17.2 Time Constants for Active Systems

The membrane time constant τ_m is a widely used measure of the dynamics of neurons. For a single RC compartment or an infinite, homogeneous cable, τ_m is simply RC. But—as discussed at length in Sec. 3.6.1—complexities arise when one considers extended passive structures. In general, for a passive compartmental model of a cell, a finite number of distinct equalizing time constants τ_i can be defined (Eq. 3.49).

These can be evaluated directly, without solving the cable equation, by efficient matrix inversion techniques (see Appendix C; Perkel, Mulloney, and Budelli, 1981). Usually, it is difficult to infer more than the first two or three (at best) of these time constants from the voltage record (e.g., Fig. 3.12). The amplitude and distribution of these time constants are related in interesting ways to the neuronal geometry and its possible symmetries. (For a

detailed discussion see Rall and Segev, 1985; Rall et al., 1992; Holmes, Segev, and Rall, 1992; Major, Evans, and Jack, 1993a,b; Major, 1993.)

A more problematic issue is the fact that real neurons show a passive response only under very limited conditions. Usually, one or more voltage-dependent membrane conductances are activated around V_{rest}. For instance, a mixed Na^+/K^+ current I_{AR} becomes activated upon *hyperpolarization*, counter to the action of most other conductances which activate upon depolarization. The action of this *anomalous* or *inward rectifier* (Chap. 9) is to reduce R_{in} and τ_m as the membrane is hyperpolarized (e.g., Spruston and Johnston, 1992). Figure 17.4 illustrates this in an exemplary way in an intracellular recording from a superficial pyramidal cell (Major, 1992). Hyperpolarizing the membrane potential from -62 to -112 mV reduces the slowest decay time constants by a factor of 3 (from 21.5 to 6.9 msec) and the input resistance by a factor of 2 (from 88.7 to 37.1 MΩ).

One possibility for obtaining the "true" value of the voltage-independent components would be to block all contaminating ionic currents by the judicious use of pharmacological channel blockers. Yet this hardly corresponds to the natural situation of a neuron receiving synaptic input.

The problem is, of course, that one cannot associate a single time constant with an active voltage-dependent membrane. Most researchers neglect this observation and fit an exponential to portions of the voltage tail of the cell's response to small current pulses (Fig. 17.4; Iansek and Redman, 1973; Durand et al., 1983; Rall et al., 1992). This yields

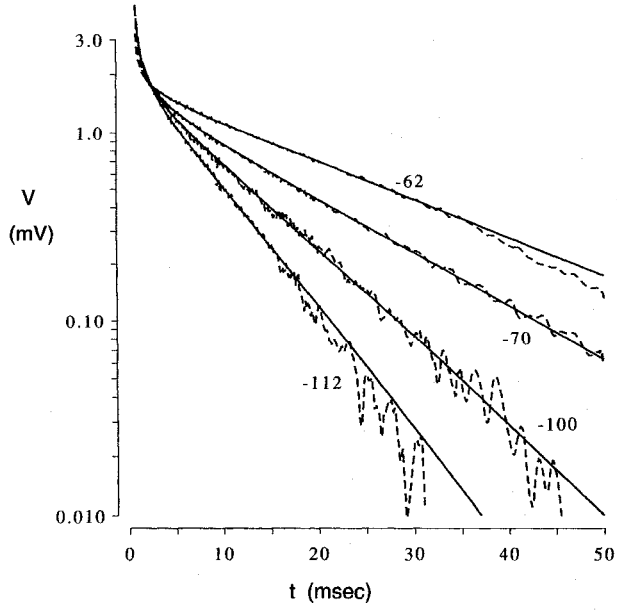

Fig. 17.4 VARIABLE MEMBRANE TIME CONSTANT Experimental record from a layer 2 pyramidal cell in the visual cortex of a rat brain slice taken by a sharp intracellular electrode. Shown is the membrane potential in response to a very short current pulse on a semilogarithmic scale at four different holding potentials. The solid lines correspond to the voltages reconstructed by "peeling" the experimental waveforms (Sec. 3.6.1). As the membrane is depolarized from -62 to -112 mV, the slowest decay—corresponding to τ_m—decreases from 21.5 to 6.9 msec, a reduction by a factor of 3. This fact makes the exact determination of a passive time constant difficult. Reprinted by permission from Major (1992).

estimates of τ_m of between 14 and 16 msec for the pyramidal cell model at rest, matching the observed time constant of 23 msec for this cell recorded in the anesthetized cat reasonably well. In the following chapter we will study how up or down regulating the synaptic input can change τ_m by an order of magnitude or more.

17.3 Action Potential Generation and the Question of Threshold

Throughout the previous chapters, we always assumed that the criterion for spike initiation is that the membrane potential exceeds a particular threshold value. To what extent is this simple assumption warranted? After all, it could well be possible that the threshold needs to be breached within a certain time window or that even further conditions, such as a minimal current, need to be fulfilled. We will now investigate this question in more detail for a membrane patch model. The more involved question of threshold generation in active cable structures is picked up in Chap. 19.

But first a preamble dealing with the instantaneous current-voltage relationship and related matters. Much of this section is based on material from Noble and Stein (1966) and Koch, Bernander, and Douglas (1995).

17.3.1 Current-Voltage Relationship

In order to understand under what conditions the cell can be thought of as having a voltage or a current threshold, we need to reconsider the steady-state current-voltage relationship $I_\infty^{\text{static}}(V_m)$ (Fig. 17.1) as well as the momentary or *instantaneous* I–V curve, denoted by $I_0(V_m)$ (Jack, Noble, and Tsien, 1975; Fig. 17.5). Numerically, this is obtained by instantaneously moving the somatic membrane potential from its resting value to a new value and assuming that all active conductances remain unchanged with the notable exception of the fast sodium activation particle m. Given the very fast time constant of sodium activation, m is practically always at equilibrium with respect to the voltage, while all other conductances have not had time to change from their values at V_{rest}.

In the subthreshold domain, both the steady-state and the instantaneous curves have very similar shapes. For the pyramidal cell model of Fig. 3.7, both currents possess the same intersection with the zero current axis at V_{rest}, are outward (positive) for more depolarized potentials, and become negative around −48 mV. However, the steady-state current quickly becomes positive again, attaining very large values. This large outward current is almost exclusively carried by the noninactivating delayed rectifying potassium current, I_{DR}, which overshadows the inactivating I_{Na}. Conversely, the instantaneous current remains negative until it reverses close to the sodium reversal potential of 50 mV. This current is dominated by I_{Na}, though with increasing depolarization the driving potential of the potassium currents and the anomalous rectifier current increase while the driving potential of I_{Na} decreases.

17.3.2 Stability of the Membrane Voltage

If the transient activation and inactivation of currents throughout the dendritic tree are neglected, the firing behavior of the cell can be defined by the nonlinear and stationary I–V curve, $I = I_\infty^{\text{static}}(V_m)$ (Fig. 17.5) in parallel with a membrane capacity. If a current I_{clamp} is injected into this circuit,

$$C\frac{dV_m}{dt} = I_{\text{clamp}} - I_\infty^{\text{static}}(V_m) \tag{17.4}$$

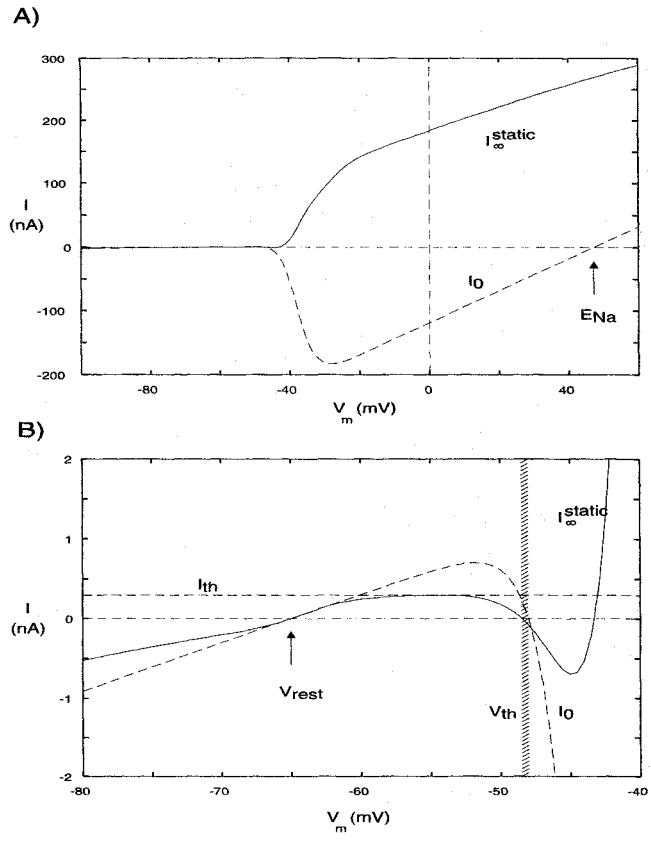

Fig. 17.5 STEADY-STATE AND INSTANTANEOUS CURRENT-VOLTAGE CURVES **(A)** Somatic membrane potential V_m was voltage clamped and the steady-state current $I_\infty^{\text{static}}(V_m)$ (same as in Fig. 17.1) at the soma of the pyramidal cell was recorded. The instantaneous I–V curve $I_0(V_m)$ is obtained by instantaneously displacing the membrane potential from V_{rest} to V_m and measuring the initial current. All somatic membrane conductances retain the values they had at V_{rest}, with the sole exception of the fast sodium activation process—due to its very fast time constant (50 μsec) we assume that it reaches its steady-state value at V_m. Note the very large amplitudes of I_0 (due to I_{Na} activation) and I_∞^{static} (due to I_{DR} activation). I_0 crosses over close to the reversal potential for I_{Na}. **(B)** Detail of **A** in the vicinity of the resting potential and spike threshold. Both curves reverse at V_{rest}. The slope of I_∞^{static} corresponds to the input (slope) conductance rest. Both curves cross zero at around −48 mV. The amplitude of $I_\infty(V_m)$ at the local peak around −54 mV represents the current threshold I_{th} for spike initiation, while the location of the middle zero crossing of I_0 corresponds to the voltage threshold V_{th} for spike initiation (indicated by the thin stippled area). Reprinted by permission from Koch, Bernander, and Douglas (1995).

determines the dynamics of the somatic membrane potential. Different from the phase space models treated in Chap. 7, this system has a single independent variable V_m and the associated phase space consists of a line. Its equilibrium points are defined by $I_{\text{clamp}} = I_\infty^{\text{static}}(\overline{V}_m)$. In the absence of an externally injected current, these are given by the zero crossings of Fig. 17.1. However, not all of these points are stable. In a manner analogous to Sec. 7.1.2, we analyze their stability by considering small variations of the membrane potential δV around these singular points $\overline{V}_m$. This leads to

$$C\frac{d\delta V}{dt} = -\frac{dI_\infty^{\text{static}}}{dV}\delta V\,. \tag{17.5}$$

In other words, in regions where the *slope conductance* $dI_{\infty}^{\text{static}}/dV$ is positive, the dynamics follow an equation of the type $\delta\dot{V} = -\alpha\delta V$ (with $\alpha > 0$) and the system will settle down to the equilibrium point (that is, $\delta V \rightarrow 0$). Under steady-state conditions, $I_{\infty}^{\text{static}}$ shows three zero crossings, one at V_{rest}, one around -48.5 mV, and one at -43 mV. The slope at the leftmost zero crossing is positive, implying that V_m at V_{rest} is stable to small perturbations. Displacing the system by $\delta V > 0$ away from V_{rest} causes a positive, outward ionic current to flow, a current that will drive the membrane potential back to V_{rest}. Conversely, a hyperpolarizing deflection will lead to an inward current that will tend to repolarize the soma.

By the same logic, the second equilibrium point at -48.5 mV is not stable. If the membrane is displaced by $\delta V_m < 0$ away from this point, a positive, outward current will flow, causing the membrane potential to decrease and to move further from this zero crossing until the system comes to rest at V_{rest}. If $\delta V_m > 0$, an inward current will flow, which further depolarizes the system. Since the smallest voltage perturbation will carry V_m away from this zero crossing, this point is unstable.

The rightmost zero crossing at -43 mV is never attained under physiological conditions, since for these values of V_m, $I_{\infty}^{\text{static}}$ lies in a realm of phase space not accessible to the system under normal conditions.

17.3.3 Voltage Threshold

To understand the origin of the voltage threshold, we make use of very simple considerations discussed more fully in Noble and Stein (1966) and Jack, Noble, and Tsien (1975). We assume that the somatic membrane receives a rapid and powerful current input caused, for instance, by numerous highly synchronized excitatory synaptic inputs (as in Fig. 17.6A) and we neglect the extended cable structure of the neuron.

This has the effect of charging up the membrane capacitance very rapidly, thereby displacing the voltage to a new value without, at first, affecting any other parameters of the system. In the limit of an infinitely fast input, the system moves along the instantaneous I–V curve I_0. If the input is small enough and displaces the potential to between V_{rest} and -48 mV, I_0 will be outward, driving the membrane potential toward less depolarized values and ultimately back to V_{rest}. This voltage trajectory corresponds to a subthreshold EPSP.

If, however, the input pulse takes V_m instantaneously beyond the zero crossing at -48 mV, I_0 becomes negative, driving the membrane to more depolarized values. In a positive feedback loop, this will further increase the inward current. The net effect is that the membrane depolarizes very rapidly: the membrane generates an action potential (Fig. 17.6B). Because during this time the other membrane currents will have started to change, I_0 can no longer be used to determine the subsequent fate of the potential. Nonetheless, the zero crossing of the instantaneous I–V curve determines the voltage value at which the membrane is able to generate sufficient current to drive the action potential without further applied current. We therefore identify this zero crossing of the instantaneous I–V curve with the voltage threshold for spike initiation V_{th} (about -48 mV).

Our argument predicts that any somatic current—whether delivered via an electrode or via synaptic input—that is sufficiently fast and powerful to depolarize the somatic membrane beyond V_{th} will initiate an action potential. We confirmed this by plotting in Fig. 17.6A the somatic potential $V_m(t)$ in response to rapid, synchronized synaptic input to the dendritic tree that is sufficient to fire the cell at a brisk rate of 21 Hz. Figure 17.6B shows a single spike in response to a brief but strong current pulse injected directly into

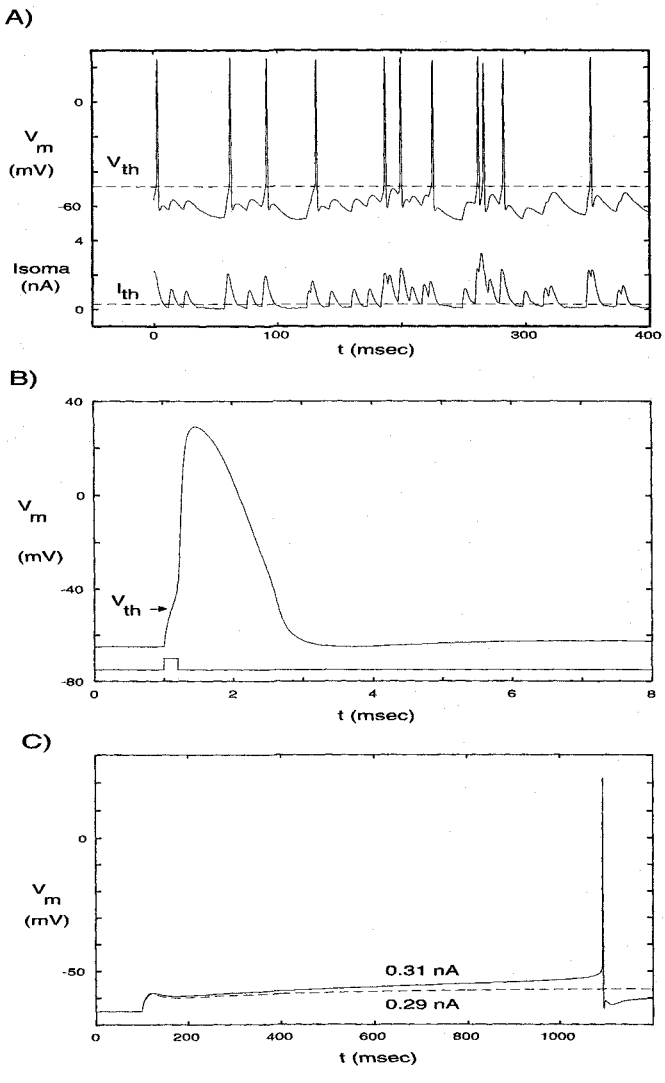

Fig. 17.6 Different Paths to Spike Initiation Generation of a somatic spike in the pyramidal cell model can occur in different ways, depending on the dynamics of the input. **(A)** Somatic voltage trace in response to random synaptic input to the dendritic tree. 100 fast (t_{peak} = 0.5 msec) AMPA synapses fired synchronously according to a Poisson process at a rate of 75 Hz. The current I_{soma} delivered by this synchronized synaptic input to the cell body is plotted at the bottom. This current was measured by clamping the soma to V_{rest} and measuring the clamp current. Even though I_{th} is frequently transiently exceeded by a large amount, the somatic membrane potential is usually not sufficiently depolarized to exceed V_{th} and initiate a spike. The variability in the amplitude of the EPSCs derives from the fact that following each synchronized synaptic event, a new set of 100 excitatory synapses is randomly chosen. A single action potential in response to **(B)** a 0.2-msec 10-nA current pulse (indicated in the lower trace) and **(C)** a sustained current step. For I_{clamp} = 0.29 nA the potential levels out at −56.5 mV, while for 0.31 nA a spike occurs with a delay of 1 sec. The first two plots demonstrate conditions under which action potentials are generated if a voltage threshold V_{th} is exceeded, while the last plot corresponds to a paradigm where spike initiation occurs if a current threshold I_{th} is exceeded. Reprinted by permission from Koch, Bernander, and Douglas (1995).

the soma. Careful inspection of both voltage trajectories indicates that each and every time $V_m(t)$ reaches $V_{th} = -48$ mV, an action potential is initiated (see dotted lines and the arrow in Fig. 17.6A, B).

Figure 17.6A reveals that many somatic EPSPs fail to trigger spikes. This fact can be exploited to operationalize the voltage threshold by histogramming the peak values of subthreshold somatic EPSPs. If spike initiation truly occurs at V_{th}, such a histogram should show peak EPSP amplitudes up to V_{th}, followed by an abrupt absence of any local maxima in V_m until, at high values, the peak voltages of the action potential itself appear. This is exactly the distribution seen in Fig. 17.7, with a complete lacuna of any local peaks in the somatic membrane potential between −48.5 and +20 mV.

This histogram was obtained using rapid synaptic input. Slow[1] synaptic input will not lead to such a crisp threshold. Experimentally, using rapid and powerful synaptic input that hovers around threshold should optimize the conditions for detecting a voltage threshold using this technique.

17.3.4 Current Threshold

Figure 17.6C illustrates a different path along which spikes can be initiated. If a small, sustained current I_{clamp} of 0.29 nA current is injected into the soma, the somatic membrane potential responds with a slight overshoot, due to the activation and subsequent inactivation of the transient A current, before settling to a steady-state somatic potential (at −56.5 mV). Increasing I_{clamp} by 20 pA is sufficient to initiate an action potential 1 sec after the onset of the current input. The extended delay between input and spike is primarily caused by I_A, as shown by Connor and Stevens (1971a,b,c). As a consequence, the cell can spike at very low frequencies (Fig. 9.7).

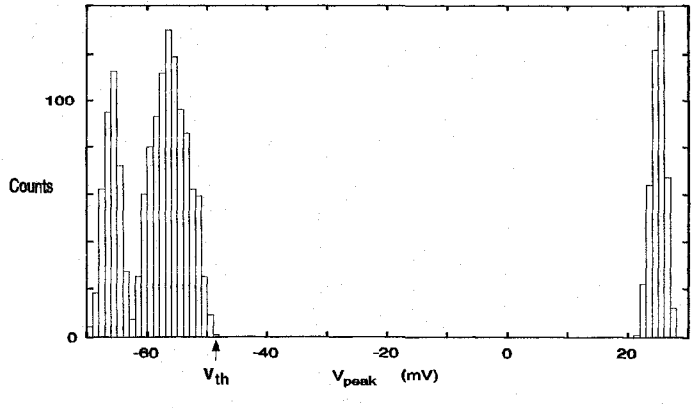

Fig. 17.7 Operationalized Definition of a Voltage Threshold The pyramidal cell model was bombarded for 20 sec with fast excitatory synaptic input (of the type shown in Fig. 17.6A, with the cell firing at 21 Hz) and the amplitude of the local maxima of the somatic membrane potential histogrammed. The three peaks correspond to the noisy synaptic background around $V_{rest} = -65$ mV (leftmost peak), synchronized EPSPs that failed to elicit action potentials (central peak), and action potentials (rightmost peak). The maximum value of the central hump is −48.6 mV, providing a convenient way in which the voltage threshold V_{th} can be measured. Reprinted by permission from Koch, Bernander, and Douglas (1995).

1. Fast and slow is always relative to the dynamics of the large sodium current determining spike initiation.

From an operational point of view, if the current delivered to the somatic membrane varies very slowly, the membrane can be thought of as having a current threshold $I_{th} = 0.295$ nA. To explain this, we turn to the steady-state I–V plot in Fig. 17.5. Injecting a sustained and depolarizing current step of amplitude I_{clamp} into the soma corresponds to shifting the I_{∞}^{static} curve downward by an equal amount. If I_{clamp} is small, the principal effect of this is to move the location of the zero crossings of I_{∞}^{static}. In particular, the leftmost zero crossing—and therefore the new somatic resting potential— shifts to the right and the middle zero crossing shifts to the left. At a critical value of I_{clamp}, labeled I_{th}, the two zero crossings merge. At this point the system still has an equilibrium point. If the current is increased any further, this portion of the I_{∞}^{static} curve drops below zero and loses its equilibrium. The inward current generated by the system forces the membrane to depolarize, driving V_m toward E_{Na} and initiating an action potential. In fact, for sustained current injections the membrane has no stable equilibrium point, displaying instead a stable limit cycle: as long as the suprathreshold current persists, the membrane generates a series of spikes. From these considerations we predict that the current threshold corresponds to the local maximum of the I_{∞} curve, here equal to 0.295 nA, very close to the value obtained by integrating the appropriate equations (Fig. 17.6C).

Note that the steady-state somatic membrane potential at which threshold current is reached (about −54.2 mV) is *different* from V_{th} because of the nonlinear and nonstationary somatic membrane. In a linear and stationary system, such as in integrate-and-fire models (Eq. 14.9) a linear relationship holds between the two,

$$V_{th} = R_{in} I_{th} . \tag{17.6}$$

17.3.5 Charge Threshold

Hodgkin and Rushton (1946; see also Noble and Stein, 1966) proposed that the threshold condition for the excitation of a cable is that a constant amount of charge Q_{th} be applied. Is this true for our cell?

When a significant amount of current—either from synaptic input or from a microelectrode—is very rapidly delivered to the cell body, the voltage change will primarily be determined by the capacitive current, since the membrane currents take time to change. Under these conditions, the cell should also show a *charge threshold*. In order to understand this, let us follow a train of thought laid out by Noble and Stein (1966). Because we are considering rapid events, the steady-state I–V in Eq. 17.4 must be replaced by the instantaneous I–V curve:

$$C\frac{dV_m}{dt} = I_{clamp} - I_0(V_m) \tag{17.7}$$

(as before, we here neglect the dendritic tree). By rearranging and integrating with respect to voltage, we obtain an expression for how long the current step has to be applied (from $V_{rest} = 0$) until the voltage threshold has been reached,

$$T_{pulse} = C \int_0^{V_{th}} \frac{dV_m}{I_{clamp} - I_0(V_m)} . \tag{17.8}$$

The integration can be carried out for any I–V relationship that does not depend on time, such as I_0 or I_{∞} (Fig. 17.5). If for short times, the injected current I_{clamp} is much bigger than the subthreshold ionic currents I_0 (on the order of 1 nA or larger; see Figs. 17.5A and 17.6), I_0 can be neglected. The total charge delivered by a step current of amplitude I_{clamp} and duration T_{th} is

$$Q = I_{\text{clamp}} T_{\text{pulse}} \approx C V_{\text{th}} = Q_{\text{th}} . \tag{17.9}$$

Put differently, for short, intense stimuli, a constant charge Q_{th} must be supplied to the capacitance in order to reach threshold (Noble and Stein, 1966).

We numerically evaluate this for a reduced one-compartment model of the pyramidal cell (Koch, Bernander, and Douglas, 1995) as well as for the full model by injecting I_{clamp} current into the soma and recording the duration of the pulse T_{pulse} necessary to generate an action potential. This threshold charge is plotted in Fig. 17.8 as a function of the amplitude of the injected current step. For the one-compartment model Q starts out high but decreases rapidly and saturates at $Q_{\text{th}} = 7.65$ pC.

If a 7.65 pC charge is placed onto a 0.508 nF capacitance (its value in the one-compartment model), the potential changes by 15.1 mV, very close to V_{th}. We conclude that in a single-compartment active model, a charge and a voltage threshold both imply the same thing: for rapid input the cell spikes whenever the input current dumps Q_{th} charge onto the capacitance, bringing the membrane potential to V_{th}. The existence of a charge threshold immediately implies an inverse relationship between the amplitude of the applied current and T_{th}. It is known that both the Hodgkin–Huxley equations for a clamped axon and the actual space-clamped giant squid axon membrane give rise to such a *strength-duration* curve (Hagiwara and Oomura, 1958; Cooley and Dodge, 1966; Noble and Stein, 1966).

This simple story becomes more complicated when we repeat the same experiment in the 400 compartment model (Fig. 17.8). The amount of charge delivered by the electrode that is necessary for the cell to spike decreases monotonically with increasing current. It only flattens out for unphysiologically large amplitudes. Under these conditions, no single

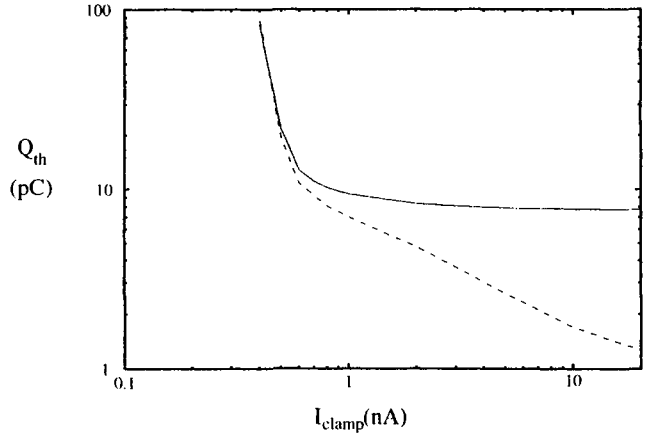

Fig. 17.8 Is There a Charge Threshold for Spiking? Relationship between the charge Q_{th} injected by a current pulse of constant amplitude I_{clamp} and duration T_{pulse} necessary for spiking to occur. For a single-compartment model of the pyramidal cell (where the effect of the entire passive dendritic tree is mimicked by adjusting the capacitance and the leak resistance at the soma), Q_{th} rapidly reaches an asymptote (solid line). That is, for moderately strong current inputs a spike is initiated whenever the limiting charge Q_{th} is delivered to the capacitance; this charge obeys $Q_{\text{th}} = CV_{\text{th}}$. In other words, for a single compartment the existence of the voltage threshold for spiking is equivalent to a charge threshold. For weaker inputs more charge is required. No such constant threshold condition is observed for the full pyramidal cell model (dashed line). Due to the presence of the distributed capacitances in the dendritic tree, action potential initiation does not obey a charge threshold condition.

equation governing the evolution of the somatic membrane potential can be written because of the presence of the many equalization time constants between the soma and the dendritic compartments. Only if the current injection is very large, with the associated very short durations <0.05 msec, can one neglect the dendritic capacitance and observe a fixed Q_{th}. We conclude that in any cell with a substantial dendritic tree, the occurrence of an action potential is not caused by the charge at the spike initiating zone exceeding some fixed threshold value.

17.3.6 Voltage versus Current Threshold

An *advocatus diaboli* might argue that the cell always possesses a voltage threshold, with the value of this threshold increasing from −48 mV for very fast inputs to −54.2 mV for slow ones. Yet in our eyes a single, but variable threshold is conceptually less elegant than two fixed but different thresholds (V_{th} and I_{th}). Furthermore, given the very broad, local peak of I_{∞}^{static} in Fig. 17.5B, V_{th} is ill defined, in particular in the face of ever existing noise.

As we will see in the following chapter, the number of simultaneously activated somatic EPSPs needed to trigger a spike is within 10% of the number predicted based on V_{th}. As long as the synaptic current delivered to the soma I_{soma} has a fast rise time compared to the activation and inactivation time constants of all the somatic currents with the exception of sodium activation (that is, on the order of 1 msec) and is powerful enough to displace V_m past V_{th}, the cell will spike. To what extent synaptic input approximates such behavior or can be better described by a slowly varying current input under *in vivo* physiological conditions depends on many factors beyond the scope of this chapter.

We are not arguing that every neuron must have I–V curves that are qualitatively similar to the ones in our model of a pyramidal cell. For instance, the steady-state I–V curve for the Hodgkin–Huxley membrane patch model is a monotonically increasing function of V_m with no local maxima (Fig. 6.9A). In this case $I_{\infty}^{static}(V_m)$ cannot be used to predict I_{th}. The instantaneous I–V curve I_0 of a patch of squid axon around rest (Fig. 6.6) does, on the other hand, look qualitatively similar to the $I_0(V_m)$ curve of the pyramidal cell and so can be used to estimate in a qualitative manner V_{th} (see Sec. 6.3.1).

17.4 Action Potential

We would be remiss if, after this extensive discussion of the conditions under which spikes can be initiated, we would not describe the action potential itself. Its form is highly stereotypical, with little variation from one spike to the next (Fig. 17.6). The spike amplitude from threshold at −49 mV to the peak at 30 mV is about 80 mV, and the full width at half height is 0.9 msec. These numbers compare favorably with experimentally recorded spikes from slice and *in vivo* (Bindman and Prince, 1983; Spain Schwindt, and Crill, 1990, 1991; Hirsch and Gilbert, 1991; Pockberger, 1991). The rapid upstroke during the initial part of the action potential, on the order of several hundred millivolts per millisecond, is caused by the sodium-mediated inward current charging up the membrane capacitance. The smaller the capacitance (as, for instance, in small cells) or the larger the density of fast, sodium channels, the faster the upstroke and, ultimately, the steeper the slope of the discharge curve. Ultimately, it is the amplitude of the upstroke that limits the speed with which action potentials can be generated.

Two ionic currents are the primary culprits in generating and shaping the action potential. The largest is the current supporting the action potential itself I_{Na} peaking at 70 nA. Due to

adaptation, peak I_{Na} for consecutive spikes is reduced to 50 nA. The second largest current is the delayed-rectifier potassium current, I_{DR} coming in at 23 nA. The gargantuan size of these two ionic currents, compared to anything the synapses in the dendritic tree can deliver to the soma, explains the almost complete independence of the shape of the action potential to the way in which the spike was triggered. The total calcium current flowing is miniscule compared to I_{Na}. Its primary function is not to drive the action potential itself but to activate calcium-dependent potassium currents controlling adaptation.

17.5 Repetitive Spiking

Until now, we have only considered the events leading to a single action potential. Yet, cells usually spike repeatedly. The response of the full pyramidal cell model to a sustained current injection is shown in Fig. 17.9. Similar to the modified Morris-Lecar equations (Eqs. 7.16 and 7.17; see also Figs. 7.10 and 7.11) and different from the squid giant axon, the pyramidal cell model can fire at very low frequencies: injecting 0.31 nA of sustained current causes the cell to spike about once every second. The current responsible for these very long interspike intervals is the inactivating potassium current I_A (Connor and Stevens, 1971a,b,c; Getting, 1989; for a detailed discussion see Fig. 9.7 and related text). Due to its hyperpolarizing reversal potential, this potassium current reduces the evoked depolarization (see the bump in Fig. 17.2). Because I_A inactivates with increasing depolarization, different from the large, delayed rectifier potassium current, it gradually decreases in size, enabling V_m to slowly creep upward until threshold is reached.

17.5.1 Discharge Curve

If the input is powerful enough to trigger two or more spikes, the firing frequency adapts within 50 msec to between one-half and one-third of its initial value. Adaptation can be

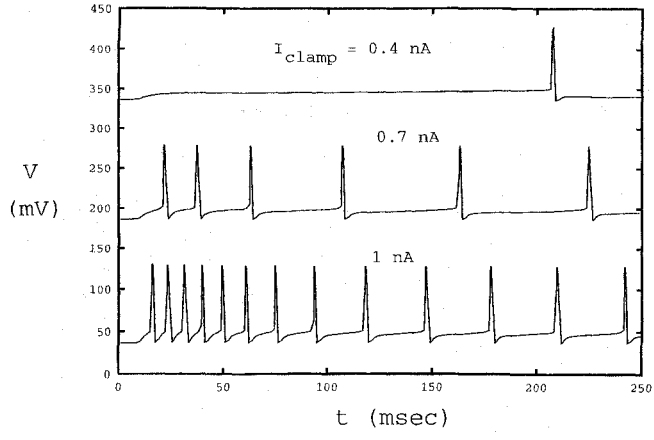

Fig. 17.9 Repetitive Firing Generation of several action potentials in the pyramidal cell model in response to sustained current injections at the cell body. The minimum current step that evokes a spike, rheobase, is $I_{th} = 0.295$ nA. Injecting 0.4 nA evokes repetitive spikes with very long interspike intervals, caused by the presence of the transient I_A current. At higher spiking frequencies, the firing adapts due to the calcium-dependent potassium currents. The voltage curves are shifted for viewing purposes. No noise has been simulated, approximating the situation one would encounter in cultured cells. Reprinted in modified form by permission from Bernander (1993).

visualized as reducing the gain of the f–I curve (Fig. 17.10A; see also Fig. 14.2C). As discussed in Sec. 9.2.2, it is caused by one or more calcium-dependent potassium currents, acting as a sustained negative input that offsets the positive current delivered via the electrode. At a very low spiking frequency, no adaptation occurs since $[Ca^{2+}]_i$ decays to its resting levels prior to the next occurrence of a spike.

The curve for the first ISI shows a biphasic shape. Initially, the slope is low from I_{th} to around 0.6 nA (*primary slope*). For larger input currents the slope is much larger (*secondary slope*). This portion of the f–I curve can be fitted rather well by a logarithmic relationship between f and I (Figs. 6.10 and 17.10A), as first observed for the uniformly polarized Hodgkin-Huxley equations (Agin, 1964). The firing frequency associated with the second ISI displays a very similar pattern, except that the primary slope spans a larger current range.

Though the shape of the adapted f–I curve in Fig. 17.10A appears deceptively linear, the slope varies by more than a factor of 2. Figure 17.10A shows the linear fit:

$$f = 49.5 \cdot (I - 0.22) \tag{17.10}$$

with the constant of proportionality corresponding to about 50 spikes per second per nanoampere of injected current, in good agreement with experimental *in vitro* (Mason and Larkman, 1990) and *in vivo* (Jagadeesh, Gray, and Ferster, 1992) observations in cat cortex. The figure also shows a logarithmic fit,

$$f = 75 \cdot (\ln I + 0.59)\,. \tag{17.11}$$

This fit is somewhat more accurate, except at very low input currents. While the difference between these two fits may seem negligible, the logarithmic fit will be more useful in the following.

Note that the discharge curve does *not* show any strong evidence of saturation in the firing frequency, a saturation that is a key property of almost all nonlinear neural network models. It is in any case unclear from where, under physiological conditions, synaptic currents greater than 2 nA would originate.

17.5.2 Membrane Potential during Spiking Activity

How can the somatic membrane potential be characterized while the system is spiking repeatedly, that is, moving along its stable attractor? A very useful heuristic measure is the time-averaged somatic membrane potential

$$\langle V_m \rangle = \frac{1}{T} \int_0^T V_m(t) dt \tag{17.12}$$

where T includes several interspike intervals in response to a sustained current I. In order to avoid the confounding effects of adaptation, $\langle V_m \rangle$ should be evaluated only after adaptation is complete. Plotting $\langle V_m \rangle$ as a function of I (solid curve in Fig. 17.10B) results in a curve with a linear relationship close to the resting potential, whose inverse slope is identical to the cell's input conductance.

Conceptually—as well as by visual inspection—this curve naturally falls into two sections. Below the point at which the cell ceases to spike and the curve shows a cusp, that is, for $I < I_{th}$, it becomes identical to the inverse of the steady-state I–V curve (Fig. 17.5B). The portion of the $\langle V_m \rangle$ versus I curve that lies beyond I_{th} shows two remarkable features. Firstly, the dynamic range of $\langle V_m \rangle$ over the physiological range of input currents is small.

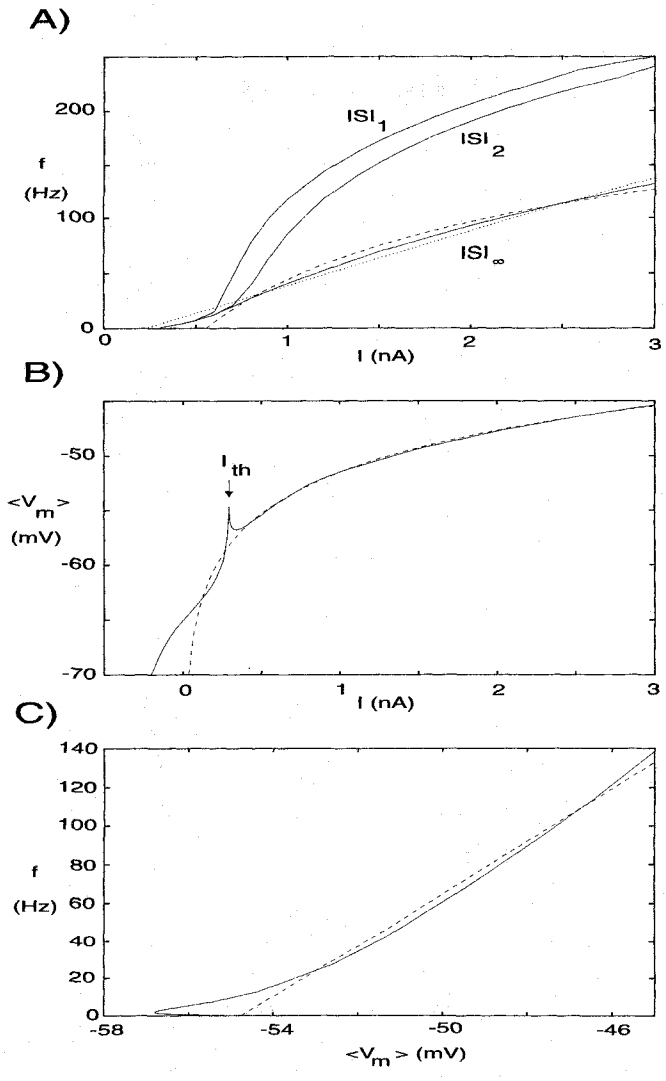

Fig. 17.10 Discharge Curve and Averaged Membrane Potential Characterization of the firing behavior of the pyramidal cell model. **(A)** Discharge curve computed as the inverse of the first, second, and fully adapted interspike intervals (solid) as a function of the amplitude of the current step (see also Fig. 14.2C). Linear (dotted) and logarithmic (dashed) fits are shown for the steady-state curve (Eqs. 17.10 and 17.11). **(B)** Introducing the averaged somatic membrane potential $\langle V_m \rangle = (1/T) \int_0^T V_m(t)dt$ enables the definition of a *dynamic I–V* relationship between a sustained input current and $\langle V_m \rangle$ (solid line). For $I < I_{\text{th}}$, this curve coincides with the conventionally defined inverse of the $I_\infty^{\text{static}}(V_m)$ curve (Fig. 17.5). The dashed curve is a logarithmic fit, indicating a diodelike relationship between the average membrane voltage and the current. **(C)** Relationship between $\langle V_m \rangle$ and the output spike frequency. Remarkably, the total dynamic range of $\langle V_m \rangle$ is only about 12 mV for physiological firing frequencies. The dashed line indicates the best linear fit (Eq. 17.15). Reprinted by permission from Koch, Bernander, and Douglas (1995).

As the adapted output spike frequency f ranges from 5 to 150 Hz, $\langle V_m \rangle$ is confined to a fairly limited range of about 12 mV. Secondly, the upper portion of the curve can be fitted very well by a logarithmic relationship, except for the "hook" around I_{th} (dashed curve in Fig. 17.10B).

This relationship can also be viewed with $\langle V_m \rangle$ as the independent variable. From this perspective, the current I can be thought of as a *cumulative spike current*, and the I–$\langle V_m \rangle$ curve as a *dynamic I–V* relationship $I_\infty^{\text{dynamic}}(\langle V_m \rangle)$ (dynamic because the somatic membrane potential travels on a stable limit cycle in response to the sustained input) that reverses at V_{rest}. $I_\infty^{\text{dynamic}}(\langle V_m \rangle)$ is quite distinct from $I_\infty^{\text{static}}(V_m)$. In the latter, the membrane potential is clamped to V_m and the current flowing at this voltage is evaluated, while in the dynamic case, a sustained current is injected while the membrane is left free to spike. The dynamic I–V curve is relatively straightforward to measure experimentally.

The logarithmic relationship implies a *diodelike* behavior, with the current depending exponentially on the average membrane potential,

$$I_{\text{spike}} = e^{(\langle V_m \rangle + 51.5)/5.50} \tag{17.13}$$

(where V_m is expressed in units of millivolts; dashed line in Fig. 17.10B). In analogy to the steady-state slope conductance $G_{\text{in}}^{\text{static}}$ (Eq. 17.3), we can define the *dynamic input conductance* as

$$G_{\text{in}}^{\text{dynamic}} = \frac{1}{R_{\text{in}}^{\text{dynamic}}} = \frac{dI_\infty^{\text{dynamic}}}{d\langle V_m \rangle} = \frac{dI_{\text{spike}}}{d\langle V_m \rangle} \tag{17.14}$$

(Fig. 17.11B). The cumulative effect of all currents active during spiking resembles a voltage-gated hyperpolarizing conductance that shunts large input currents, thereby stabilizing the membrane potential. In the absence of this "spike" current the membrane would depolarize to much higher values. For instance, with an input conductance of $G_{\text{in}}^{\text{static}} = 60.6$ nS at V_{rest}, a 2 nA injected current step should depolarize the membrane to -34 mV in the absence of any active currents, while the actual potential $\langle V_m \rangle$ is approximately -48 mV. We conclude that the dynamic conductance $G_{\text{in}}^{\text{dynamic}}$ acts similarly to an imperfect voltage clamp, providing a stable sink for currents originating in the dendrites, a rather unusual way to look at the spike generation mechanism (Koch, Bernander, and Douglas, 1995).

Finally, we can combine the logarithmic relationship between injected current and firing frequency (Eq. 17.11) with the exponential dependence of I_{spike} on $\langle V_m \rangle$ (Eq. 17.13) to arrive at a linear relationship between the averaged membrane potential and the firing frequency,

$$f(\langle V_m \rangle) = 13.6 \cdot (\langle V_m \rangle + 54.8). \tag{17.15}$$

This relationship is useful for analog electronic circuit implementation of neurons (Mahowald and Douglas, 1991; Douglas, Mahowald, and Mead, 1995), since it allows one to interpret the membrane potential across some transistor as an effective firing frequency without adding additional circuitry to implement some output nonlinearity. As can be seen in Fig. 17.10C, the true spike frequency curve (as ascertained from the simulations) lies above Eq. 17.15 for small firing frequencies. Before concluding, several remarks pertinent to the definitions of these dynamics variables are in order.

1. The low-pass nature of the dendritic tree, caused by the distributed capacitance, will filter out the high-frequency components associated with the rapid up and down swing

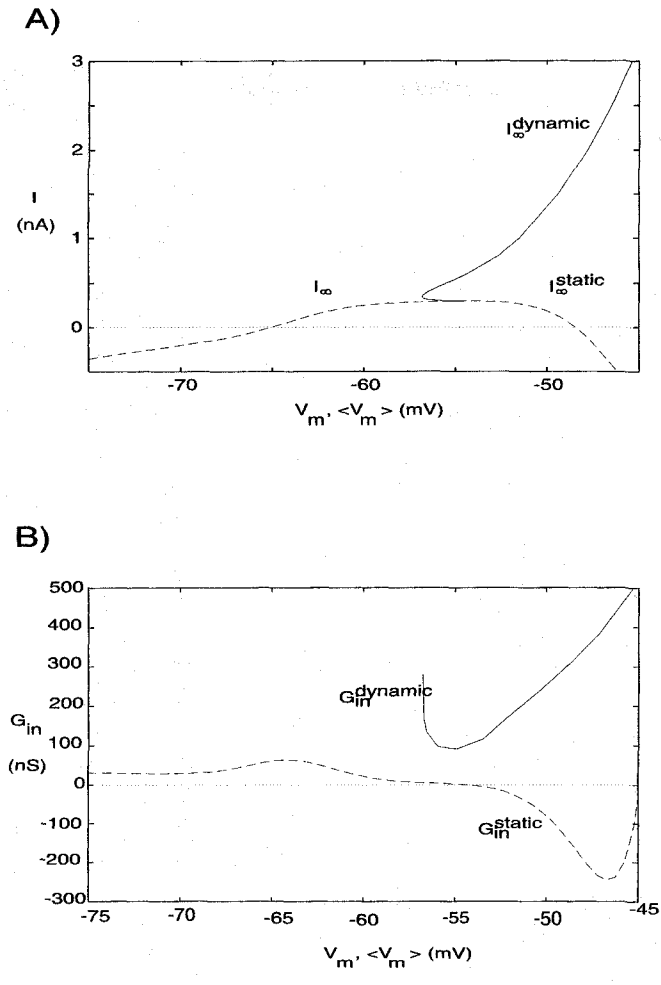

Fig. 17.11 Dynamic Discharge Curve Time-averaged membrane potential $\langle V_m \rangle$ permits the introduction of a dynamic I–V curve as the relationship between the average somatic membrane potential in the full pyramidal cell model and the total current flowing across the somatic membrane. **(A)** The static I–V curve is computed under *voltage* clamp by measuring the clamp current and its dynamic counterpart under *current* clamp (it is the inverse of the curve in Fig. 17.10B). In the subthreshold regime $I < I_{\text{th}}$ the two curves coincide (labeled I_∞). **(B)** The sustained and dynamic somatic input conductances as a function of V_m or $\langle V_m \rangle$ defined as the slopes of the I–V curves in **A**. For $V < V_{\text{th}}$, $G_{\text{in}}^{\text{dynamic}} = G_{\text{in}}^{\text{static}}$. The dynamic input conductance allows the introduction of a time constant that characterizes how rapidly the adapted firing rate responds to new input. Reprinted by permission from Koch, Bernander, and Douglas (1995).

of the action potentials as they propagate from the soma into the apical tree. Thus, $\langle V_m \rangle$ is qualitatively closer to the membrane potential seen by dendritic sites than $V_m(t)$. Also, slowly activating or inactivating conductances do not care about rapid fluctuations in V_m, but are responsive to a low-pass filtered or average potential.

2. $I_\infty^{\text{dynamic}}(\langle V_m \rangle)$, in combination with the cell's discharge curve, leads to a linear relationship between the average membrane potential $\langle V_m \rangle$ and the firing rate in the fully adapted case (Eq. 17.15).

3. The time-averaging technique discussed here represents one way in which the dynamics of a complex neuron can be reduced to the mean-field dynamics of the standard neural network unit (Sec. 14.4). It is not advisable to use $\langle V_m \rangle$ when considering fast events that depend on the exact timing (e.g., fast dendritic spikes discussed in Sec. 19.3).

4. The ratio of the membrane capacitance and $G_{\text{in}}^{\text{dynamic}}$ can be thought of as a *dynamic time constant* τ_{dynamic}. It is a measure of how rapidly the averaged membrane potential, and therefore the firing rate, can vary in response to a change in I_{soma}. As can be seen in Fig. 17.11B, if sufficient current is injected for the cell to fire in a sustained manner at 65 Hz, $\langle V_m \rangle = -50$ mV, increasing $G_{\text{in}}^{\text{dynamic}}$ by about a factor of 4 relative to rest. This implies that the effective time constant of the cell has decreased to about 4 msec. Due to the presence of the many membrane conductances generating and modulating action potentials, the firing rate can respond much faster to a rapid increase in I_{soma} than suggested by the conventional definition of τ_m. For higher firing rates, τ_{dynamic} can be close to 2 msec, implying that neurons can respond at the millisecond or faster scale (Softky, 1994). Whether cells make use of this very high bandwidth is another matter.

Our enthusiasm for such a new measure must be tempered by two considerations. First, the $I_{\infty}^{\text{dynamic}}(\langle V_m \rangle)$ curve is defined for the adapted firing frequency, and adaptation takes between 20 and 100 msec to occur. A second difficulty is that τ_{dynamic} is defined for a fictive, continuous firing rate and for a constant current input. This is a meaningless quantity on a time scale less than the interspike interval. This sampling problem renders the exact definition of a time course problematic at very low firing frequencies.

17.6 Recapitulation

This chapter treated the characterization of a nonlinear and nonstationary neuron from the point of view of the soma on the basis of two measures: the relationship between the current flowing across the somatic membrane and the voltage and the local slope of such an I–V curve. The inverse of this last variable is the slope or input resistance. The traditional I–V curve $I_{\infty}^{\text{static}}(V_m)$ is defined under voltage clamp conditions: the voltage is fixed and the current flowing at this voltage is recorded. The local peak around V_{rest} defines the minimal current I_{th} necessary to initiate spiking. Under the assumption that the activation and inactivation variables of the voltage-dependent currents change much more slowly than the activation $m(t)$ of the sodium current, it is possible to define an instantaneous current-voltage curve $I_0(V_m)$. (Conceptually, this can be measured by yanking the membrane potential from V_{rest} to V_m and instantaneously recording the resulting membrane current.) Stability considerations of the sort explored in Chap. 7 dictate that the zero crossing of I_0, if the slope is negative, corresponds to the voltage V_{th} that needs to be exceeded for a spike to occur.

We conclude that *fast* and *powerful* versus *sustained* but *peri-threshold* stimuli define two different threshold conditions: in the first case V_m must exceed V_{th} while in the latter case I_{soma} must exceed I_{th}. The larger the current delivered to the soma by a synaptic input, the faster V_{th} can be reached and the sooner the cell spikes. This process is not limited by τ but by the amplitude of the upstroke of the action potential (that is, by the amout of sodium current and the somatic capacitance). For cells with no or little distributed capacitances, that is, with small dendritic trees, a voltage threshold is equivalent to a charge threshold, in

which a fixed amount of charge needs to be placed onto the somatic capacitance in order to reach V_{th}.

Introducing $\langle V_m \rangle$ as the temporal average of the somatic membrane potential (including spikes) allows us to extend most of the above concepts into the spiking regime. Biophysically, $\langle V_m \rangle$ approximates the average membrane potential experienced by a distal dendritic site, where the high-frequency components of the back-propagating somatic action potential have been filtered out by the capacitances distributed throughout the cable.

The dynamic current-voltage curve $I_{\infty}^{\text{dynamic}}(\langle V_m \rangle)$ is defined as the inverse of the relationship between the sustained current injected via a microelectrode and the average membrane potential (Koch, Bernander, and Douglas, 1995). It can be thought of as a single, effective *spike* current that serves to stabilize the membrane potential in the neighborhood of V_{th} and that reverses at V_{rest}. This current can be described rather well by an exponential relationship: increasing $\langle V_m \rangle$ by 3.7 mV roughly doubles I. The fact that this current behaves similarly to a diode in the forward direction makes such a relationship particularly easy to implement using electronic circuits. A similar exponential relationship also exists for a patch of squid axon described by the Hodgkin–Huxley equations (not shown).

One caveat. These dynamical measures are based on time-averaged quantities; they cannot be used under conditions where the detailed time course of spiking is thought to be relevant for postsynaptic processing.